Acta Materialia 131 (2017) 315–322

Contents lists available at ScienceDirect

Acta Materialia

journal homepage: www.elsevier.com/locate/actamat

Full length article

Reactive diffusion and stresses in nanowires or nanorods

Manuel Roussel [a, *], Zoltán Erdélyi [b], Guido Schmitz [a]

[a] Institute of Materials Science, University of Stuttgart, Heisenbergstraße 3, D-70569, Stuttgart, Germany
[b] Department of Solid State Physics, University of Debrecen, P. O. Box. 400, H-4002, Debrecen, Hungary

ARTICLE INFO

Article history:
Received 23 January 2017
Accepted 2 April 2017
Available online 5 April 2017

Keywords:
Reactive diffusion
Stress
Core-shell
Nanowires

ABSTRACT

Heterostructured nanowires are of prime interest in nowadays technology such as field-effect transistors, field emitters, batteries and solar cells. We consider their aging behavior and developed a model focusing on reactive diffusion in core-shell nanowires. A complete set of analytical equations is presented that takes into account thermodynamic driving forces, vacancy distribution, elastic stress and its plastic relaxation. This complete description of the reactive diffusion can be used in finite element simulations to investigate diffusion processes in various geometries. In order to show clearly the interplay between the cylindrical geometry, the reactive diffusion and the stresses developing in the nanowire, we investigate the formation of an intermetallic reaction product in various core-shell geometries. Emphasis is placed on showing how it is possible to control the kinetics of the reaction by applying an axial stress to the nanowires.

1. Introduction

In Ref. [1] we presented a complete set of analytical equations to describe reactive diffusion in spherical core shell nanostructures. The model takes into account elastic stress, its plastic relaxation, as well as possible non-equilibrium vacancy densities. Furthermore, thermodynamic driving forces are included to model the formation of intermetallic (IM) product phases within an intermediate composition range. Using this model, we studied the reaction in spherical triple core-shell structures *A/B/A* and *B/A/B*, for which Schmitz et al. [2] observed that the growth rate depends on the stacking order. Comparison with the data of atom probe tomography (APT) proved that significant deviations from the vacancy equilibrium concentration develop over time which control stability and reaction rate of the nanometric diffusion couples.

In this paper, we will present a new set of analytical equations, this time to describe reactive diffusion in a *cylindrical* core shell nanostructure. The interest in the cylindrical geometry stems from the ever growing importance of nanowires, nanowhiskers and nanopillars in recent technologies as they are used in new generation of devices or prototypes in numerous fields: field-effect transistors [3,4], battery electrodes [5,6], flexible solar cells … [7]. For such applications, homogeneous nanowires are not sufficient. More elaborate structures, such as core-shell nanowires, are often necessary. If the core shell structure is lost, for example upon heating, the function also deteriorates. Consequently, knowledge about reaction of layers and the developing-relaxing stress field is indispensable to prevent this deterioration and to construct more stable structures.

Basic equations describing the reactive diffusion in cylinders are developed in the following. We will then use computer simulation in order to solve this set of equations. Various examples will help us discuss the interplay between diffusion, elastic stress, plastic relaxation and vacancy concentration. In addition, we will show that applying external forces on the wires allows controlling the reaction: either accelerate or decelerate the process, enhance or hinder the formation of an intermixed phase as desired.

2. Basic equations

In order to keep the analytical formulas transparent, we will refer to isotropic elasticity. As it was pinpointed by Beke et al. in Ref. [8], the creation of a new phase with a different specific volume from the parent phases during reactive diffusion induces a stress-free strain. This stress-free strain, in turns, plays a major role in the kinetics of the process. Therefore, our model needs to describe the stress-free expansion and plastic deformation as it was already discussed in Refs. [1,9]. Stress-free expansion is supposed to be isotropic; accordingly, it has the form $\varepsilon_{ik}^{SF} = \varepsilon^{SF}\delta_{ik}$ (δ_{ik} is the unit tensor). In plastic deformation, volume remains constant, i.e.

* Corresponding author.
E-mail address: manuel.roussel@gmail.com (M. Roussel).

http://dx.doi.org/10.1016/j.actamat.2017.04.001
1359-6454/

$\mathrm{tr}\widehat{\varepsilon}^P = 0$; i.e. plastic deformation is anisotropic, but it can be supposed that all the non-diagonal elements of the tensor $\widehat{\varepsilon}^P$ are equal to zero, therefore its components can be expressed as $\varepsilon^P_{ik} = \varepsilon^P_{ik}\delta_{ik}$. Thus, the stress induced by the creation of a new phase after plastic relaxation can be written as

$$\sigma_{ik} = \frac{E}{(1+\upsilon)(1-2\upsilon)}\{[(1-2\upsilon)\varepsilon_{ik} + \nu\varepsilon_{ll}\delta_{ik}] - \left[(1+\upsilon)\varepsilon^{SF} + (1-2)\nu\varepsilon^P_{ik}\right]\delta_{ik}\} \quad (1)$$

using the Einstein's summation convention. In terms of displacement ($\vec{u}$), the equation of equilibrium in the case of internal stress-free strain is

$$\frac{1-\nu}{1+\nu}\,\mathrm{grad}\,\mathrm{div}\vec{u} - \frac{1-2\nu}{2(1+\nu)}\mathrm{rot}\,\mathrm{rot}\vec{u} = \mathrm{grad}\varepsilon^{SF} + \frac{1-2\nu}{1+\nu}\mathrm{div}\widehat{\varepsilon}^P \quad (2)$$

where ν is Poisson's ratio, E is Young's modulus.

3. Solution of the equation of equilibrium in the case of a fixed cylinder

In order to mimic the conditions of a core-shell nanowire, we solved the equation of equilibrium assuming a cylindrical symmetry. The wire is also considered fixed at both ends and can be stressed initially in the axial direction (the solution for a free wire is given in Appendix A). This specific geometry implies the following: only the radial component u of the dilatation vector differs from zero (azimuthal and axial components $u_\theta = u_z = 0$). Consequently eq. (2) has the following form in cylindrical coordinates

$$\frac{1-\nu}{1+\nu}\left[\frac{1}{r}\frac{\mathrm{d}(ru)}{\mathrm{d}r}\right] = \frac{\mathrm{d}\varepsilon^{SF}}{\mathrm{d}r} + \frac{1-2\nu}{1+\nu}\left[\frac{\mathrm{d}\varepsilon^P_{rr}}{\mathrm{d}r} + \frac{1}{r}\left(\varepsilon^p_{rr} - \varepsilon^p_{\theta\theta}\right)\right] \quad (3)$$

Here the indices "rr" and "θθ" denote the radial and the azimuthal components of the tensors. Applying axial force to the wire initially and fixing its ends under this stressed state, the solution of the equilibrium equation is

$$u = \frac{1-\nu}{1+\nu}\frac{1}{r}\int_{R_i}^{r} r\left[\varepsilon^{SF} + \frac{1-2\nu}{1+\nu}\left(\varepsilon^P_{rr} + A\right)\right]\mathrm{d}r + C_1 r + \frac{C_2}{r} - \nu\frac{C_3}{E}r \quad (4)$$

where

$$A = 2\int_{R_i}^{r}\frac{\varepsilon^P_{rr}}{r}\mathrm{d}r \quad (5)$$

C_1, C_2 and C_3 are constants of integration to be determined from boundary conditions and R_i is any convenient lower limit for the integral, such as inner radius of a hollow cylinder or $R_i = 0$ for a solid cylinder. Eq. (4) has been obtained using $\mathrm{tr}\widehat{\varepsilon}^P = 0$. Since the wire is fixed at both ends $\varepsilon^P_{zz} = 0$ and $\varepsilon^P_{rr} = -\varepsilon^P_{\theta\theta}$. Note that without any axial initial force, the term $-\nu\frac{C_3}{E}r$ vanishes. Therefore, this term considers that the displacement is affected by the uniform initial stress applied.

Knowing the displacement vector, the components of the total strain tensor in cylindrical coordinates can be determined using $\varepsilon_{rr} = \mathrm{d}u/\mathrm{d}r$, $\varepsilon_{\theta\theta} = u/r$ and $\varepsilon_{zz} = \mathrm{d}u_z/\mathrm{d}z$ [10]. For these we obtain

$$\begin{aligned}
\varepsilon_{rr} &= \frac{1+\nu}{1-\nu}\left\{-\frac{1}{r^2}\int_{R_i}^{r} r\left[\varepsilon^{SF} + \frac{1-2\nu}{1+\nu}\left(\varepsilon^P_{rr} + A\right)\right]\mathrm{d}r + \varepsilon^{SF} + \frac{1-2\nu}{1+\nu}\left(\varepsilon^P_{rr} + A\right)\right\} + C_1 - \frac{C_2}{r^2} - \nu\frac{C_3}{E}\\
\varepsilon_{\theta\theta} &= \frac{1+\nu}{1-\nu}\frac{1}{r^2}\int_{R_i}^{r} r\left[\varepsilon^{SF} + \frac{1-2\nu}{1+\nu}\left(\varepsilon^P_{rr} + A\right)\right]\mathrm{d}r + C_1 + \frac{C_2}{r^2} - \nu\frac{C_3}{E}\\
\varepsilon_{zz} &= C_3/E
\end{aligned} \quad (6)$$

The components of the stress tensors can then be obtained by substituting the strain components in eq. (1):

$$\begin{aligned}
\sigma_{rr} &= -\frac{E}{1-\nu}\frac{1}{r^2}\int_{R_i}^{r} r\left[\varepsilon^{SF} + \frac{1-2\nu}{1+\nu}\left(\varepsilon^P_{rr} + A\right)\right]\mathrm{d}r + \frac{E}{1+\nu}\left(A + \frac{C_1}{1-2\nu} - \frac{C_2}{r^2}\right)\\
\sigma_{\theta\theta} &= \frac{E}{1-\nu}\frac{1}{r^2}\int_{R_i}^{r} r\left[\varepsilon^{SF} + \frac{1-2\nu}{1+\nu}\left(\varepsilon^P_{rr} + A\right)\right]\mathrm{d}r - \frac{E}{1-\nu}\varepsilon^{SF} + \frac{E}{1+\nu}\left(\frac{\varepsilon^P_{rr}}{1-\nu} + \frac{\nu}{1-\nu}A + \frac{C_1}{1-2\upsilon} + \frac{C_2}{r^2}\right)\\
\sigma_{zz} &= -\frac{E}{1-\nu}\varepsilon^{SF} + \frac{\nu E}{1+\nu}\left(\frac{\varepsilon^P_{rr} + A}{1-\nu} + \frac{2}{1-2\nu}C_1\right) + \frac{1-\nu}{(1+\nu)(1-2\nu)}C_3
\end{aligned} \quad (7)$$

The constants of integration can now be determined using the boundary conditions. For instance, in the case of a solid cylinder ($R_i = 0$) with free outer surfaces ($\sigma_{rr}(R_o) = 0$) the displacement at the center of the cylinder is equal to zero: $u(R_i) = 0$. Thus, it follows from eq. (4) that

$$C_2 = 0 \quad (8)$$

By definition C_3 is the uniform axial stress applied initially, so

$$C_3 = \sigma^0_{zz} \quad (9)$$

Moreover, since the cylinder is free to expand in the radial direction, the radial component of the stress tensor vanishes at the

outer surface: $\sigma_{rr}(R_o) = 0$, where R_o denotes the radius of the outer surface of the cylinder. Combining this boundary condition with the first of eq. (7) and eq. (8), we obtain the following expression for C_1:

$$C_1 = \frac{(1+\nu)(1-2\nu)}{1-\nu}\frac{1}{R_o^2}\times\int_{R_i}^{R_o} r\left[\varepsilon^{SF} + \frac{1-2\nu}{1+\nu}\left(\varepsilon_{rr}^{P} + A\right)\right]\mathrm{d}r - (1-2\nu)A(R_o) \tag{10}$$

4. Thermodynamics, diffusion and associated stress-free volume change (ε^{SF})

The above theory provides us with the necessary tools to handle any kind of internal stress-free volume change and plastic relaxation. As it was already described in Ref. [1] ε^{SF} can be determined during a solid state reactive diffusion experiment. In general, it is necessary to distinguish between volume transport caused by mere diffusion and volume transport caused by deformation (convection) arising from imbalanced partial diffusional fluxes, creation/annihilation of vacancies and change in specific volume by reaction. Similarly to what has been done in the case of nanospheres in Ref. [1] the stress-free volume change can be determined for a core-shell nanowire:

$$\frac{\mathrm{D}\varepsilon^{SF}}{\mathrm{D}t} = -\frac{1}{3}\left\{\frac{1}{r'}\sum_{i=1}^{n}\frac{\partial}{\partial r'}\left[r'(\Omega_i - \Omega_v)j_i\right] - q\right\} \tag{11}$$

Given this specific geometry, fluxes only flow in the radial direction. Here D/Dt is the *substantial (or material) derivative*. It gives the rate change of any scalar quantity seen at a point which follows the motion of the material coordinate system. It is related to the time derivative in the spatial coordinate system by $Da/Dt = \partial a/\partial t + \vec{v}\nabla a$. Moreover, Ω_i is the atomic volume of component i, and Ω_v is the volume of a vacancy. The prime denotes that the calculation of the stress-free change of a volume element is done in the material coordinate system, and q is the relative change in volume caused by creation/annihilation of vacancies and change in specific volume [1]. By integrating this equation, it is possible to follow ε^{SF} over time.

4.1. Calculation of the fluxes $\vec{j}_i$

The flux of component i can be written as [1,9]

$$\vec{j_i} = -\rho\frac{\mathscr{D}}{kT}c_i c_v \nabla'\left[\left(\mu_i^{SF} + \Omega_i P\right) - \left(\mu_v^{SF} + \Omega_v P\right)\right] \quad \text{for i} = 1,\ldots,\text{n}, \tag{12}$$

in which we have conveniently defined $\mathscr{D}_i = D_i^*/c_v^0$, with D_i^* being the tracer diffusion coefficient of the chemical component i [1,11]; k and T are Botzmann's constant and the absolute temperature. Furthermore, μ_i and μ_v are the chemical potentials of the component i and of the vacancies respectively. P is the pressure. ρ is the total material density (number of lattice sites per volume) and can be calculated from the partial material densities of the components i (ρ_i) and that of the vacancies ρ_v: $\rho = \sum_{i=1}^{n}\rho_i + \rho_v$. c_i and c_v^0 are the atomic fraction of component i and of the vacancy in equilibrium; atomic fractions are related to the material densities by

$$c_i = \frac{\rho_i}{\rho}\,\text{for i} = 1,\ldots,\text{n and i} = v. \tag{13}$$

4.2. Chemical driving forces

In the following examples, we consider a binary system *A-B*. The corresponding free enthalpy curves have been tuned to lead to the formation of only one intermetallic phase B_2A. These conditions have been chosen close to the observation in many experiments regarding reactive diffusion in nanostructures. Usually, only a single intermetallic is formed in early reaction stages and this phase in general does not reveal a symmetric *AB* composition. For instance in the experiments described in Ref. [2], the authors studied reactive diffusion in *Cu-Al* diffusion couples where only the formation of Al_2Cu was observed.

The Gibbs energy of mixing of an ideal binary solid solution (SS) is natural, while the Gibbs energy of the intermetallic phase (IM) is approximated by a second order polynomial:

$$\begin{aligned} g^{SS} &= kT[c\ln c + (1-c)\ln(1-c)] \\ g^{IM} &= -g_0 + V(c-c_m)^2 \end{aligned} \tag{14}$$

Concerning the intermetallic phase, c_m denotes the stoichiometric concentration of component A and g_0 and V are parameters which can be adjusted in order to reflect the existence range of the intermetallic phase. Knowing this, the chemical potentials of component A for the solid solution and the intermetallic phases can easily be determined:

$$\begin{aligned} \mu_A^{SS} &= kT\ln c \\ \mu_A^{IM} &= -g_0 + V\left(-c^2 + c_m^2 + 2c - 2c_m\right) \end{aligned} \tag{15}$$

Both the free enthalpy curves and the chemical potential μ_A are displayed in Fig. 1. Existence ranges of the solid solution and the intermetallic have been determined using the double tangent method. Since in the composition ranges $0 \ldots c_1$ and $c_4 \ldots 1$ the solid solution is stable, the chemical potential is calculated from μ_A^{SS}; in the range $c_2 \ldots c_3$, the intermetallic compound is the stable phase, so μ_A is calculated from μ_A^{IM}. In the two-phase ranges $c_1 \ldots c_2$ and $c_3 \ldots c_4$, the chemical potential remains constant and equals to $\mu_A(c_1)$ and $\mu_A(c_3)$ calculated from either μ_A^{SS} or μ_A^{IM}. μ_B can be determined analogically.

4.3. Composition over time and continuity equation

In order to simulate reactive diffusion, the change of composition in time and space caused by vacancy mediated diffusion is calculated using the equation

$$\frac{\mathrm{D}c_i}{\mathrm{D}t} = -\frac{1}{\rho}\nabla'\vec{j}_i - c_i s_v \,\text{for i} = 1,\ldots,\text{n}, \tag{16}$$

for all n atomic components [1]. ∇' indicates the *divergent* calculated in the material coordinate system, and s_v gives the rate of change of the vacancy concentration due to their creation/annihilation at the sinks and sources.

For cylindrical geometry if fluxes only flow radially, eq. (16) becomes

$$\frac{\mathrm{D}c_i}{\mathrm{D}t} = -\frac{1}{\rho r'}\frac{\partial}{\partial r'}(r' j_i) - c_i s_v \tag{17}$$

4.4. Change in volume - q

We consider two contributions to q: the relative change in volume caused by creation/annihilation of vacancies (q_v) and the change in specific volume due to phase transformation (q_{sv}):

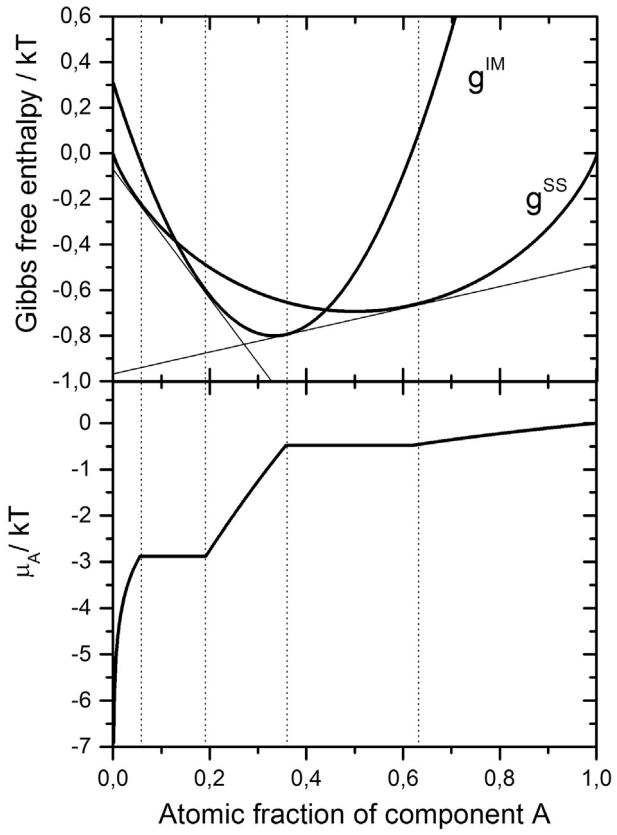

Fig. 1. Free enthalpy of mixing for a solid solution (g^{SS}) and a B_2A intermetallic (g^{IM}) phase; corresponding chemical potential for the component A is displayed in the bottom panel. ($c_m = 0.33333$, $g_0/kT = 0.8$ and $V/kT = 10$).

$$q = q_v + q_{sv} \tag{18}$$

Concerning q_v, we supposed that a pressure P changes the vacancy concentration from its unstressed equilibrium value c_v^0 to:

$$c_v(P) = c_v^0 \exp\left(-\frac{\Omega_v P}{RT}\right) \tag{19}$$

in which $P = -\frac{1}{3}\mathrm{tr}\hat{\sigma}$. The rate of vacancy creation/annihilation at a source/sink is considered to be proportional to the deviation of the current fraction of vacancies from the equilibrium one

$$s_v = K_r\left[c_v^0 \exp\left(-\frac{\Omega_v P}{RT}\right) - c_v\right] \tag{20}$$

where the rate coefficient K_r determines the effectiveness of sinks and sources. We emphasize that K_r is not necessarily a constant but may vary, for instance, with spatial coordinates depending on the spatial distribution of the sinks and sources. In the following examples, $K_r = 1$ at the outer surface of the nanowire and at the intermetallic interfaces. $K_r = 0$ everywhere else. Note that other expressions for s_v can also be used. See for instance in Refs. [12,13]. However, the present work is not intended to investigate the role of the different expressions for s_v. Knowing s_v and $c_v(P)$, q_v can be determined as:

$$q_v = s_v \rho \Omega_v \tag{21}$$

Concerning the relative change in volume due to phase transformation q_{sv}, it depends on the crystallography of the system and is an input parameter. For example, in the following, the change in specific volume for a reaction $A + 2B \rightarrow B_2A$ is chosen to be 6%, therefore $q_{sv} = 0.06$.

5. Stress relaxation via plastic deformation

Our model allows the stress created by reactive diffusion. This is achieved by enabling complete plastic relaxation in the newly created intermetallic phase. Plastic relaxation is governed by the shear part of the stress tensor. Therefore, only shear stress ($\hat{\sigma}^{shear}$) induces shear strain ($\hat{\varepsilon}^p$) or strain rate ($\dot{\hat{\varepsilon}}^p$). In the case of a large plastic deformation, the distribution of shear stress is determined by viscous flow, as follows: $\hat{\sigma}^{shear} = 2\eta\dot{\hat{\varepsilon}}^p$, where η is the shear viscosity. Accordingly,

$$\dot{\hat{\varepsilon}}^p = \frac{1}{2\eta}\hat{\sigma}^{shear} = \frac{1}{2\eta}\left(\hat{\sigma} - \frac{1}{3}\mathrm{tr}\hat{\sigma}\right) \tag{22}$$

More particularly, in the case of a cylinder geometry

$$\begin{aligned}
\dot{\varepsilon}^P_{rr} &= \frac{1}{6\eta}(2\sigma_{rr} - \sigma_{\theta\theta} - \sigma_{zz}) \\
\dot{\varepsilon}^P_{\theta\theta} &= -\frac{1}{6\eta}(2\sigma_{\theta\theta} - \sigma_{rr} - \sigma_{zz}) \\
\dot{\varepsilon}^P_{zz} &= 0
\end{aligned} \tag{23}$$

Note that $\dot{\varepsilon}^P_{zz} = 0$ stems from the fact that we are describing a nanowire which is fixed at both ends. Furthermore, even though we limit ourselves to viscous flow, other mechanisms can lead to stress relaxation and can be implemented in eq. (22).

6. Numerical calculation

In the following examples, the reactive diffusion in core-shell nanowires has been simulated. In order to calculate the radial composition and the stress profile over time, eqs. (17) and (7) must be solved along with (12), (20), (11) and (23). To this end, a finite volume method (FVM) was used. The nanowire was divided into n cylindrical shells. During each iteration, the atomic and volume fluxes between each neighboring shells are calculated. In turns, the composition, the stress and the shell thickness is updated in each cell. For a more detailed presentation of the numerical algorithm see Ref. [1].

In most cases samples were divided into 120–150 shells, however different numbers were also used to check independency of the mesh. The following input parameters were used: $R_i = 0$ in order to simulate a solid nanowire core and R_o was in the range of 45–145 nm, representing the initial radius of the wires.

Initially, the vacancies were distributed homogeneously inside the wire and usually their concentration was $c_v^0 = 10^{-3}$. Although this is much larger than in real cases, more realistic values of c_v^0 would drastically increase the computation time. Nonetheless, tests were performed with $c_v^0 = 10^{-4} - 10^{-6}$ and led to the conclusion that the value of c_v^0 did not change the results qualitatively.

$D_A^*/D_B^* = \mathscr{D}_A/\mathscr{D}_B = 0.1$ in the intermetallic phases; outside $\mathscr{D}_A = \mathscr{D}_B$. This corresponds to a typical situation. Often, the diffusivity of the majority component in an intermetallic reveils a higher mobility (Cu_3Au rule), while the partial diffusivities in a random alloys are quite close, given a vacancy mechanism of diffusion [14,15]. $\mathscr{D}_A = 1.8 \times 10^{-14}$ m^2/s; although its value does not play an important role, just scales the time. As we did not intend to fit particular experimental data, determination of the real timescale was not crucial.

In addition, atomic volumes of both species were approximated to be similar: $\Omega_A = \Omega_B = 7 \times 10^{-6}$ m^3/mol. $T = 700$ K, although in the calculations presented in this work, it does not play any role,

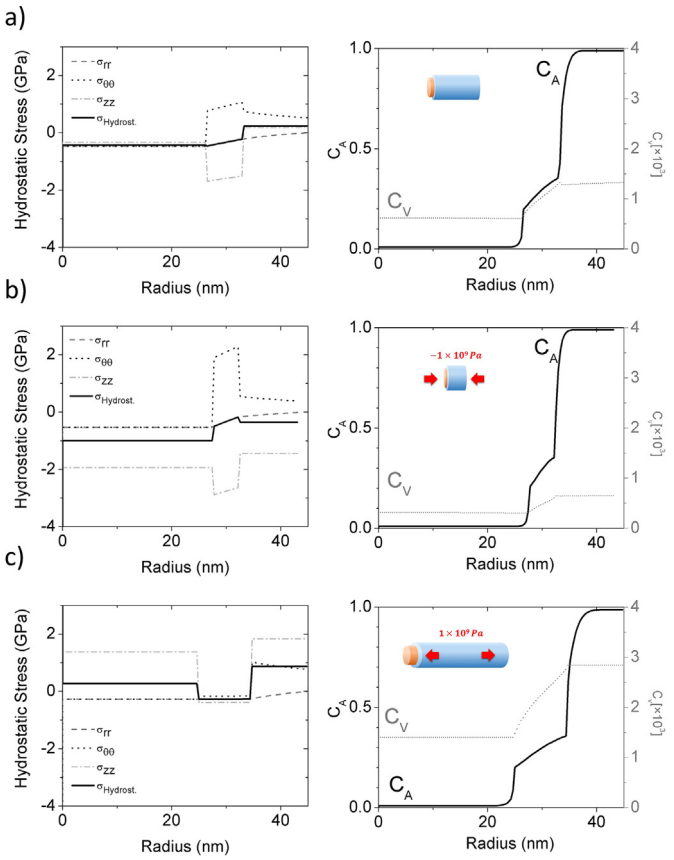

Fig. 2. Profiles of stress and composition for a *B* wire coated by an *A* layer: initially (a) stress free $\sigma^0_{zz} = 0$; (b) applying compressive $\sigma^0_{zz} = -1$ GPa; (c) applying tensile $\sigma^0_{zz} = 1$ GPa stress. Thicknesses of the grown intermetallic layer are 6, 4 and 9 nm, respectively. (The calculation time and the axises are the same for (a)–(c) for direct comparison.).

since due to the supposition $\Omega_A = \Omega_B = \Omega_v$, the only terms containing the temperature explicitly vanishe. To mimic the conditions supposed in Ref. [2], $E = 90$ GPa and $\nu = 0.345$ and the viscosity was set to 10^{100} Pa outside the intermetallic phases to prevent any relaxation, and to 10^3 Pa inside the intermetallic phases to allow complete plastic relaxation.

Finally we note that equations for free standing cylindrical wires (free ends) are given in Appendix A. In this case the algorithm is the same but the corresponding equations must be used.

7. Results and discussion

The model described above provides us with the necessary tools to study the interplay between stresses and reactive diffusion during the aging of a nanowire. First, we show results obtained for cylindrical bilayers. This simple geometry will help us to clear up the role of stresses and their possible relaxation. To this end, we have performed the following calculations for *A/B* (*A* is inside and *B* outside) and *B/A* stacking orders of the bilayer core-shell structure: i) no initial axial stress, applying ii) compressive, and iii) tensile initial stress. In all calculations, partial diffusion coefficient of the majority component *B* inside the intermetallic (B_2A superlattice structure) was 10 times higher than that of the *A* component. In all cases, the growth rate of the intermetallic layer considerably depends on the stacking sequence. In the *A/B* wires, the growth is slowed down compared to *B/A* wires in which it is accelerated. This different behavior is a direct consequence of the vacancy gradient which develops inside the wire (see Fig. 2a). As a general trend, and independently of the stacking sequence, the core of the wire gets under compressive stress and the outer part under tensile stress. This leads to the development of an increase in the vacancy concentration towards the surface of the wire. Inside the intermetallic layer, the vacancy gradient is always pointing outwards, whatever the stacking order. On the contrary, the vacancy flow generated by the difference in mobility of *A* and *B* species does depend on the stacking order and is always directed towards the *B* phase. In the case of the *A/B* wire, the vacancy flow is directed upwards the existing vacancy gradient whereas in the case of the *B/A* wire, it is directed downwards. Consequently, the growth of the intermetallic is slower for the *A/B* wire and faster for the *B/A* wire.

Fig. 2 shows that applying initial axial force to the wire influences the growth rate of the intermetallic dramatically. Compressive stress ($\sigma^0_{zz} < 0$) slows down the process, whereas tensile one ($\sigma^0_{zz} > 0$) enhances the growth as compared to the initially stress free case ($\sigma^0_{zz} = 0$). This is because the initial axial stress superposes on the developing stress field, which affects the hydrostatic stress. The change in hydrostatic stress (or pressure), controlled to a major part via the change in σ_{zz}, influences the overall vacancy concentration in the wire (see eq. (19)) which, in turns, influences the speed of the reaction. As can be seen in Fig. 2, the application of 1 GPa of axial stress changes the growth rate of the IM by about 50%. This first observation is already of prime interest, since it means that the kinetics of reactive diffusion in a nanowire could be controlled by applying an initial stress along the wire axis.

In order to point out the influence of the stacking order combined with the initial applied stress, we repeated the calculations for a trilayer core-shell nanowire; *A/B/A*. Interestingly, the intermetallic grows asymmetrically as can be seen in Fig. 3a: faster at the outer interface than at the inner interface. On the basis of the explanation for the bilayer geometry, the interpretation of these results is quite straightforward. It is, again, the distribution of the vacancies determined by the stress field, which controls the growth rate. The profile of hydrostatic stress has a stepwise character decreasing from outside to inside for both stacking orders. Accordingly, vacancy concentration also decreases towards the center. The intermetallic layer grows slower at the interface at which the direction of the gradient of vacancy concentration is opposite to the gradient of the *A* (slower) atoms. As a result, the growth rate is larger at the outer interface for the *A/B/A*.

The application of compressive initial axial stress on the wire, as expected on the basis of the results for the bilayer, will depress the growth rates but the qualitative behavior remains the same as previously described. More interestingly, when applying a tensile initial axial stress we predict a striking effect. As it can be seen in Fig. 3, the application of increasing initial tensile stress leads to different observations. First of all, the growth rate increases (Fig. 3b) as it was already the case for the bilayer. But more importantly, if the tensile stress is high enough, the asymmetry is suppressed and even reversed (Fig. 3c). The origin of this lies in the fact that the application of a rather high initial tensile stress masks the stress variations caused by reactive diffusion. Consequently, the overall gradient of the hydrostatic stress towards the free surface, which was observed in an initially stress free wire, vanishes. Diffusion kinetics is then governed by a vacancy concentration profile which is not step-like anymore, as can be observed in Fig. 3c.

Ultimately, this even leads to the inversion of the asymmetry in IM layer growth rate inside the wires. This inversion can be seen in Fig. 4. Here, we show the thickness of the grown IM layers during two different simulations: i) without initial stress $\sigma^0_{zz} = 0$; ii) applying tensile stress of $\sigma^0_{zz} = 3$ GPa. As expected, the overall kinetics of the reactive diffusion process is much faster in the case of the tensile stress due to a higher average vacancy concentration in

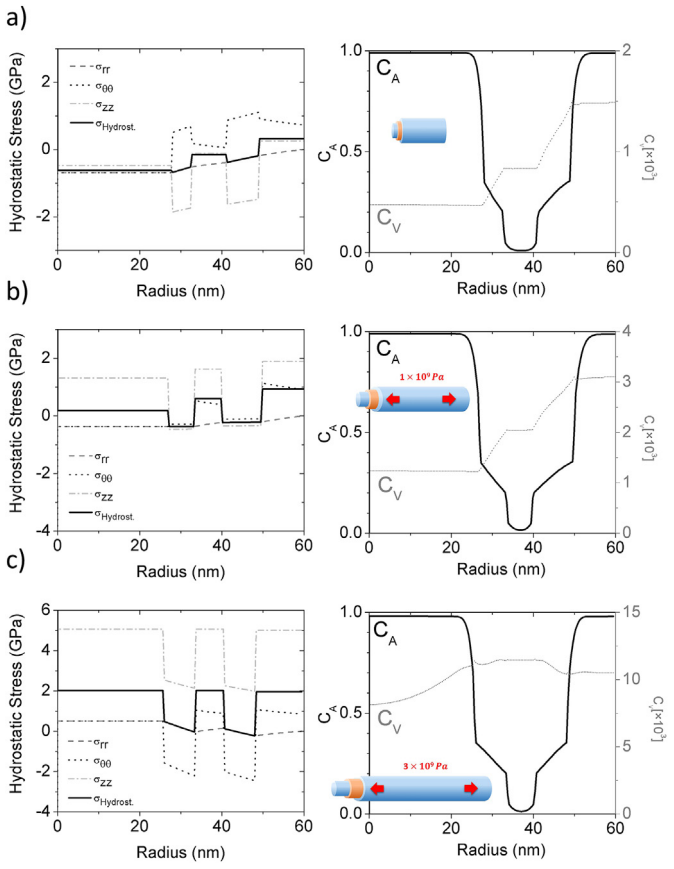

Fig. 3. Profiles of stress and composition for a *A*/*B*/*A* wire: a) initially stress free $\sigma^0_{zz} = 0$; b) applying tensile stress of $\sigma^0_{zz} = 1$ GPa, and c) $\sigma^0_{zz} = 3$ GPa. The tensile stress increases the growth rate but not only. If high enough, it can suppress the asymmetry, or even revert it in later stages (not shown here). For better comparison, the width of the outer IM is the same in all shown cases.

the whole wire. In addition, one can clearly see that in the initially stress free wire, the inner IM grows faster whereas in the tensile stress case, it is the outer IM layer which is the wider. This observation itself is of prime interest because it demonstrates how *applying stress to an ageing nanowire might be utilized to control its final microstructure*.

Finally, it is worth noting that the peculiar stress profiles developing during reactive diffusion are the consequence of the geometry of the problem. As it has already been demonstrated now, switching from a spherical geometry to a cylinder induces tremendous changes in the behavior of the IM growth. Additionally, it can be expected that with increasing the core radius of the nanowires, the observed asymmetry will decrease or even vanish (since increasing the radius will ultimately correspond to reaching a planar thin film configuration). To check this, we repeated the calculations with an increasing core radius as it is shown in Fig. 5. As expected, the asymmetry almost completely disappears for a core with a radius of 115 nm, demonstrating that the discussed effect can only be observed in nanometric structures.

We also performed this calculation for the spherical geometry (not included in Ref. [1]), which also shows, as expected, that with increasing sphere radius the peculiar behavior disappears (see Appendix A).

It is worth saying some words about the possibility of experimental verification. A suggested way to apply initial axial stress on a cylinder could be by pressing a cylindrical pillar by the tip of an atomic force microscope (AFM) or a nano indenter. The required

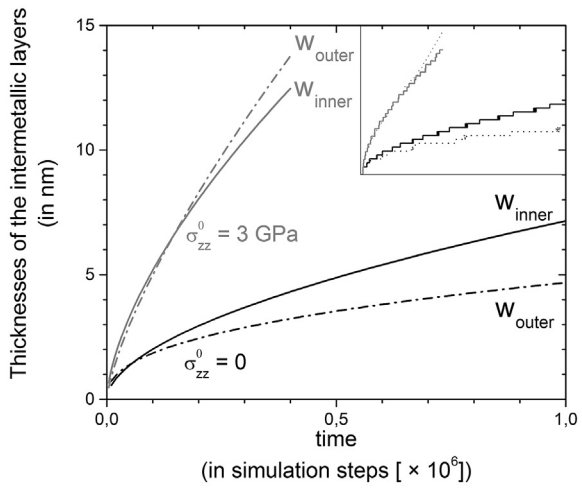

Fig. 4. Thickness of the IM layers over time for a fixed wire (black curves) and a for an initial applied tensile stress of 3 GPa (grey curves). The data has been fitted using an allometric fit, the original data which exhibits steps corresponding to the mesh of the simulations is given in the inset.

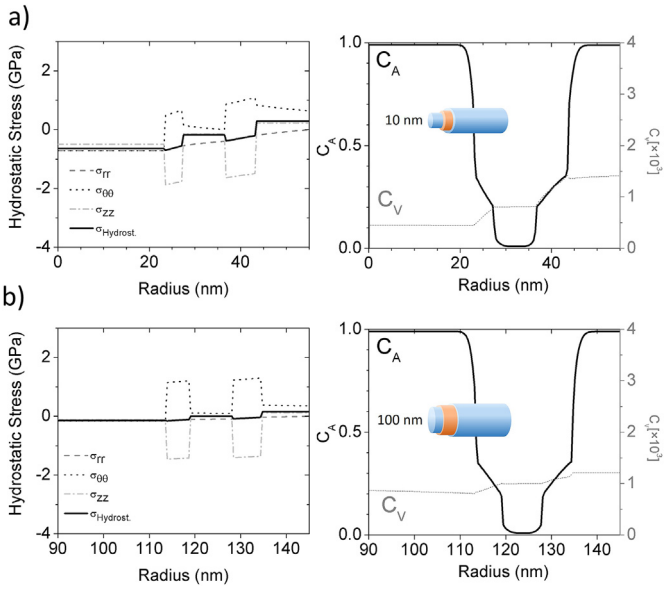

Fig. 5. Profiles of stress and composition for an *A*/*B*/*A* wire: initially stress free $\sigma^0_{zz} = 0$. The radius of the core is (a) 25 and (b) 115 nm. For case (b) the asymmetry in IM growth cannot be observed.

force to apply 1 GPa of axial stress is in the range of 5–30 μN for pillars with a radius of 40–100 nm, which is well feasible.

8. Conclusions

We studied theoretically the reactive diffusion in core-shell nanowires. A complete set of analytical equations has been developed, taking into account elastic stress caused by the formation of new phases and initial axial straining, its plastic relaxation and non-equilibrium vacancy distribution caused by imbalanced atomic fluxes, moreover the thermodynamic potentials to model the formation of an intermetallic phase in a binary alloy. This model was used to predict that elastic stresses have a tremendous influence on the growth rate of intermetallic layers in simple core-shell geometries (*A*/*B* and *B*/*A*) and more complex structures such as triple

layers (*A/B/A*).

Our first conclusion is that in an initially stress free nanowire, growth rates of the IM layers significantly depend on the stacking sequence. In the case of a positive volume excess of the reaction, the nanowires are under compressive stress in their inner part and under tensile stress towards their outer surface. This leads to an inhomogeneous vacancy distribution which hinders the outward flux of vacancies.

Second, we have shown that by applying initial axial stress to the nanowires, we may affect the IM growth. Applying a compressive stress, for instance, reduces the average vacancy concentration in the nanowires, leading to a decreased growth rate of the IM. Inversely, an initial tensile stress speeds up the process. More interestingly, for the triple layer geometry we may force the asymmetry in growth rates by applying compressive stress and suppress or even reverse it by applying tensile stress.

The simulated reactions show that it is possible to control the microstructure of a nanowire undergoing reactive diffusion just by applying initial stress to it. The developed model will also be useful to clear up the role of stress in the nowadays popular nanowires and nanotubes.

Acknowledgements

This work was supported by the Alexander von Humboldt Foundation (1153163), the OTKA Board of Hungary (NF 101329), the GINOP-2.3.2-15-2016-00041 project co-financed by the European Union and the Regional Development Fund and the German science foundation (DFG, SCHM 1182/9).

Appendix A. Free ends

If the wire is not stressed initially in the axial direction, normal force distributed according to

$$\sigma_{zz} = -\frac{E}{1-\nu}\varepsilon^{SF} + \frac{\nu E}{1+\nu}\left(\frac{\varepsilon_{rr}^{P}+A}{1-\nu} + \frac{2}{1-2\nu}C_1\right) \tag{A.1}$$

must be applied to the ends of the cylindrical wire in order to keep $u_z = 0$. If we superpose a uniform axial stress, we can choose C_3 so that the resultant force on the ends is zero

$$\int_0^{R_o} \sigma_{zz} 2\pi r \mathrm{d}r = \int_0^{R_o} C_3 2\pi r \mathrm{d}r = C_3 2\pi R_o^2 \tag{A.2}$$

Note that the self-equilibrating distribution remaining on each end will give rise only to local effects at the ends according to Saint-Venant's principle (" … the difference between the effects of two different but statically equivalent loads becomes very small at sufficiently large distances from load.") [16,17].

The stress σ_{rr} and $\sigma_{\theta\theta}$ will still be given by the first and second in eq. (7). The radial displacement and the radial and azimuthal strain components will also be given by eq. (4) and the first two of eqs. (6) and (A.2), respectively. The axial displacement and strain are, however, corresponding to the uniform stress C_3 determined from eq. (A.1) and: $\varepsilon_{zz} = C_3/E$. The constants of integration C_1 and C_2 for a solid cylinder will still be given by eqs. (10) and (8), whereas C_3

$$C_3 = \frac{2E}{1-\nu}\frac{1}{R_o^2}\int_{R_i}^{R_o} r\varepsilon^{SF}\mathrm{d}r - \frac{2\nu E}{(1+\nu)}\left[\frac{1}{(1-\nu)R_o^2}\int_{R_i}^{R_o} r\left(\varepsilon_{rr}^{P}+A\right)\mathrm{d}r + \frac{1}{1-2\nu}C_1\right] \tag{A.3}$$

Finally the axial component of the shear strain rate is

$$\dot{\varepsilon}_{\theta\theta}^{P} = -\frac{1}{6\eta}(2\sigma_{\theta\theta} - \sigma_{rr} - \sigma_{zz}) \tag{A.4}$$

Appendix B. Radius dependence for spherical geometry

Fig. B1 shows for a spherical core-shell structure that with increasing core radius the asymmetry in IM growth disappears. The core is rigid and inert, only the three layers on top react. The parameters and the algorithm were the same as in Ref. [1].

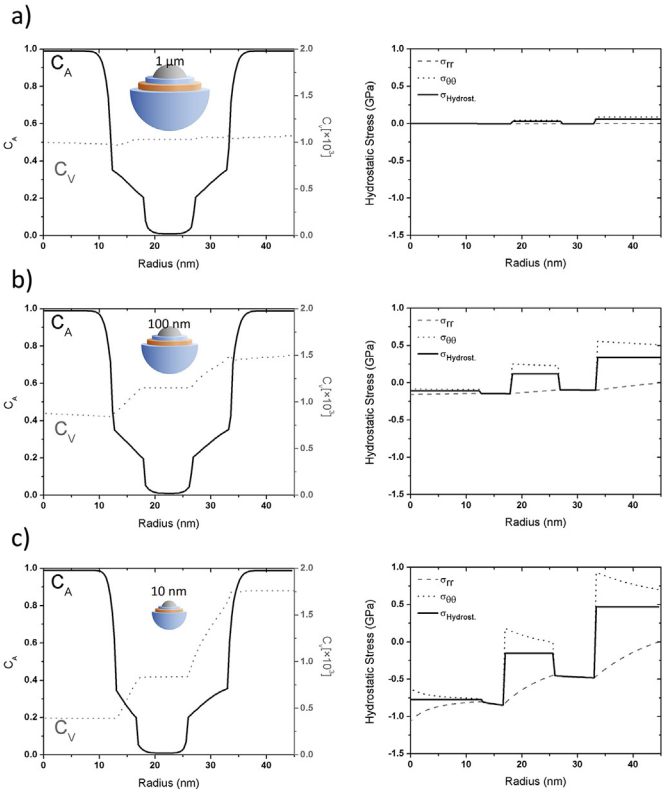

Fig. B.1. Profiles of stress and composition for an *A/B/A* layer stack on a rigid core sphere (initially stress free). Radius of the inner core a) 1 μm, b) 100~nm, and c) 10~nm. Asymmetry in growth rates of the reaction products vanishes with increasing core size.

References

[1] Z. Erdélyi, G. Schmitz, Reactive diffusion and stresses in spherical geometry, Acta Mater. 60 (2012) 1807–1817.
[2] G. Schmitz, C.B. Ene, C. Nowak, Reactive diffusion in nanostructures of spherical symmetry, Acta Mater. 57 (9) (2009) 2673–2683.

[3] Y. Hu, J. Xiang, G. Liang, H. Yan, C.M. Lieber, Sub-100 nanometer channel length ge/si nanowire transistors with potential for 2 thz switching speed, Nano Lett. 8 (3) (2008) 925–930.
[4] J. Xiang, W. Lu, Y. Hu, Y. Wu, H. Yan, C.M. Lieber, Ge/si nanowire heterostructures as high-performance field-e ect transistors, Nature 441 (7092) (2006) 489–493.
[5] L.F. Cui, R. Ruffo, C.K. Chan, H. Peng, Y. Cui, Crystalline amorphous core shell silicon nanowires for high capacity and high current battery electrodes, Nano Lett. 9 (1) (2009) 491–495.
[6] K. Takahashi, Y. Wang, G. Cao, NiV2O5 nH2O CoreShell nanocable arrays for enhanced electrochemical intercalation, J. Phys. Chem. B 109 (1) (2005) 48–51.
[7] Z. Fan, D.J. Ruebusch, A.A. Rathore, R. Kapadia, O. Ergen, P.W. Leu, A. Javey, Challenges and prospects of nanopillar-based solar cells, Nano Res. 2 (11) (2009) 829–843.
[8] D. Beke, I. Szabó, Z. Erdélyi, G. Opposits, Diffusion-induced stresses and their relaxation, Mater. Sci. Eng. A 387 (2004) 4–10.
[9] G.B. Stephenson, Deformation during interdiffusion, Acta Metall. 36 (10) (1998) 2663–2683.
[10] L.D. Landau, E.M. Lifshitz, Theory of Elasticity; vol. 7 of Course of Theoretical Physics, second ed., Pergamon Press, 1970.
[11] S.V.B. Heidelberg, Diffusion in Solids, Springer-Verlag, Berlin Heidelberg, 2007.
[12] J. Svoboda, F. Fischer, Modelling of the influence of the vacancy source and sink activity and the stress state on diffusion in crystalline solids, Acta Mater. 59 (3) (2011) 1212–1219.
[13] Y. Mishin, J.A. Warren, R.F. Sekerka, W.J. Boettinger, Irreversible thermodynamics of creep in crystalline solids, Phys. Rev. B 88 (18) (2013) 184303.
[14] F.M. D'Heurle, Nucleation of a new phase from the interaction of two adjacent phases: some silicides, J. Mater Res. 3 (1988) 167.
[15] F.M. D'Heurle, P. Gas, J. Philibert, Diffusion defect data, Pt, A, Defect Diffus. Forum vol. 529 (1997) 143–147.
[16] A.E.H. Love, A Treatise on the Mathematical Theory of Elasticity, Cambridge University Press, 1927.
[17] A.J.C.B. Saint-Venant, Memoire sur la Torsion des Prismes; Mem. Divers Savants, 1855.